Cellulose (2015) 22:1841–1852
DOI 10.1007/s10570-015-0620-4

ORIGINAL PAPER

Controlled synthesis of ZnO particles on the surface of natural cellulosic fibers: effect of concentration, heating and sonication

S. A. Ovalle-Serrano · V. S. Carrillo · C. Blanco-Tirado · J. P. Hinestroza · M. Y. Combariza

Received: 12 January 2015 / Accepted: 30 March 2015 / Published online: 8 April 2015

Abstract We report on the use of fique natural fibers as solid matrices for the deposition of zinc oxide (ZnO). Fique fibers, native to Colombia, are composed of cellulose (63–70 %) and have a heterogeneous surface morphology with high oxygen density that facilitates metal oxide nanoparticle growth and stabilization. Fique fiber–ZnO biocomposites were synthesized by a co-precipitation method using $ZnSO_4$ as precursor, NaOH for hydroxide formation and thermal/ultrasound energy to promote $Zn(OH)_2/Zn(OH)_4^{2-}$ decomposition and ZnO formation. The biocomposite was characterized using X-ray diffraction, X-ray fluorescence, Fourier transform infrared spectroscopy with attenuated total reflectance, field emission scanning electron microscopy, energy dispersive X-ray spectroscopy and X-ray photoelectron spectroscopy. The synthesis of ZnO nanoparticles has been widely reported on inorganic substrates and soft natural fibers; however studies on how experimental parameters affect ZnO features on heterogeneous phase reactions are scarce, as well as the use of hard complex cellulosic fibers as solid supports for its growth. We observed that $[OH^-]/[Zn^{2+}]$ ratios, heating or sonication time wield a strong influence on the amount, shape, size and distribution of ZnO crystals on the fique fibers; hence confirming the potential of hard natural fibers as surface active materials for novel biocomposites synthesis. We believe these materials, where the hard fiber robustness and the transition metal oxide catalytic properties are synergistically combined, could be promising functional alternatives that will favor a widespread nanoparticle usage for environmental applications such as wastewater treatment processes.

Keywords Natural fibers · Fique · Zinc oxide nanoparticles · Biocomposites

Electronic supplementary material The online version of this article (doi:10.1007/s10570-015-0620-4) contains supplementary material, which is available to authorized users.

S. A. Ovalle-Serrano · V. S. Carrillo · C. Blanco-Tirado · M. Y. Combariza (✉)
Escuela de Química, Universidad Industrial de Santander, Bucaramanga 680001, Colombia
e-mail: marianny@uis.edu.co

J. P. Hinestroza
Fiber Science Program, Cornell University, Ithaca, NY 14850, USA

Introduction

Natural hard fibers are hollow complex structures that function as support elements and transport units in plants. These fibers are natural biocomposites made up of crystalline and amorphous cellulose fibrils kept together in bundles by hemicellulose and lignin. Due to the polar nature of cellulose and its porous structure, natural fibers are currently attractive supports for deposition and stabilization of nanostructured materials, to produce functional biocomposites, by various

synthetic approaches (John and Thomas 2008; Faruk et al. 2012). These hybrid materials can be obtained by combining a wide range of cellulosic structures (whole fibers, micro- and nanofibers and nanocrystals), and nanostructured materials (noble metals, transition metal oxides, semiconductors, etc.; Barua et al. 2013; Galland et al. 2013; Katepetch et al. 2013). Applications of these materials range from energy storage, catalytic beds for pollutant capture and degradation, new membranes, smart textiles, antimicrobial elements, screens for electronic applications and magnetic products (Perelshtein et al. 2009; Xue et al. 2012; Chacón-Patiño et al. 2013; Galland et al. 2013).

Fique fibers belong, along with sisal, henequen, coir, piassava and abaca, to the group of natural hard fibers. Cellulose in fique fibers amounts up to 63 % in weight, followed by lignin with 14.5 % in weight and the remaining is composed of hemicellulose and other minor components (Gañán and Mondragon 2002). Our group previously reported on the use of these fibers as solid supports to successfully deposit and stabilize in its surface, a wide range of nanostructures such as noble metals and transition metal oxide nanoparticles (NPs; Castellanos et al. 2012; Chacón-Patiño et al. 2013).

Zinc oxide (ZnO) is known to have unique electrical, photocatalytic, optical and antibacterial properties; it is also cheap and has high surface reactivity. These properties make ZnO ideal for technological applications such as light emitting diodes, gas sensors, solar cells and photocatalytic systems (Gaya et al. 2010; Katepetch et al. 2013; Selvam et al. 2013). Many reports about the synthesis of ZnO nanoparticles using both sonochemichal and thermal methods, in homogeneous and heterogeneous phases, have been reported. For example, regarding synthesis in heterogeneous phases, Perelshtein et al. used a sonochemical method to synthesize ZnO semispherical nanoparticles ($\sim$30 nm) on cotton fibers (Perelshtein et al. 2009). Katepetch et al. (2013) deposited ZnO nanoparticles, with crystallite size of about 60 nm and cauliflower-like morphology, on bacterial cellulose pellicles using an ultrasonic-assisted in situ method. Chen et al. (2013) reported a method where bacterial cellulose, zinc acetate and diethylene glycol were heated at 170–180 °C to obtain ZnO nanoparticles with spherical shapes and diameters around 100–500 nm. Heating at 60 °C was reported as a way to synthesize ZnO structures with flower-like morphology on glass slides and silicon wafers, (Yamabi and Imai 2002). These reports show that regardless of the method used for the synthesis, the size and shape of ZnO particles mostly depend on the characteristics of the surface where they are deposited.

Most literature reports deal with the synthesis of ZnO nanoparticles in homogenous phase or in heterogeneous phase onto inorganic substrates; only very few show the synthesis of ZnO nanoparticles on cellulosic substrates, and mostly on cotton and bacterial cellulose. In this contribution we report the synthesis of the ZnO particles on the surface of hard cellulosic fibers, to our knowledge the first report of its kind. Unlike soft cellulosic fibers, these macrofibers are structurally sound, water resistant, and have a heterogeneous surface that facilitates NP size control, dispersion, and stabilization. We believe biocomposites of hard natural fibers and catalytically active nanomaterials (such as ZnO whose photocatalytic oxidation properties have been applied to contaminant degradation, particularly for water treatment processes) could be considered as the ultimate green materials because they exhibit remarkable environmental advantages such as biocompatibility, biodegradability, functionality and the ability to be reused, as we have previously demonstrated with other materials of this kind (Castellanos et al. 2012; Chacón-Patiño et al. 2013; Ovalle et al. 2014).

On the other hand, reports dealing with the influence of experimental parameters on ZnO particles size and shape are exclusively limited to homogenous phase reactions. We are interested in observing the influence of experimental conditions on liquid–solid heterogeneous systems. Hence, in this contribution we report on the influence of experimental parameters such as $[OH^-]/[Zn^{2+}]$ ratio, application of thermal or mechanical energy, and reaction time on the shape, size and distribution of ZnO nanoparticles on the surface of complex cellulosic fibers.

Experimental

Materials

Raw fique fibers were acquired from the "Fique Producers Association", Mogotes, Santander, Colombia. Zinc sulphate heptahydrate ($ZnSO_4{\cdot}7H_2O$), sodium hydroxide (NaOH) and hydrochloric acid (HCl)

were purchased from Merck (Darmstadt, Germany). All reagents were used without further purification. Aqueous solutions were prepared using deionized water (18.2 MΩ).

Fiber pretreatment and cationization

To eliminate residues, such as chlorophyll, waxes and leftover tissue from the fiber's decortication process, fique fibers were sonicated at 40 °C for 60 min in a Bransonic Ultrasonic bath (130 W, 40 kHz). Sonication also contributed to the elimination of calcium salts (such as carbonates and oxalates) commonly found in natural fibers. Alkali cellulose was produced by initially placing clean fique fibers in a 6 % HCl aqueous solution for 3 h at room temperature; after reaction the fibers were removed from the solution and washed in distilled water to be further placed in contact with a 6 % NaOH aqueous solution for 3 h, this process has been previously reported by Li and Wang (Li et al. 2007; Wang et al. 2010). After these treatments alkali cellulose is obtained, due to the formation of $–CH_2O^-Na^+$ groups on the primary OH at C-6 of the glucose units within the polymer. This material was washed in distilled water, dried at 60 °C and used as cation exchanger and as a solid support for the ZnO synthesis.

ZnO particle synthesis

We followed a modified procedure from that reported by Kawano and Imai (2006). In short, cationic fique fibers were immersed in solutions of $ZnSO_4{\cdot}7H_2O$:NaOH with $[OH^-]/[Zn^{2+}]$ molar ratios of 20:1, 10:1 and 4:1. The samples were either heated to 60 °C for 60 and 120 min, or subjected to sonication for 20 and 40 min (Azizian-Kalandaragh et al. 2009). For the sonochemical synthesis we used a low frequency/high power Ultrasonic Processor (Sonics vibra cell VC, 20 kHz, 750 W). Since it is well know that for chemical reactions (particularly in nanoparticle synthesis) the ultrasound source must not be used continuously due to solvent overheating, which affects dramatically the solvent́s surface tension and hence the cavitation process, we used an on/off pulser on the instrument that allows us to release ultrasound energy in bursts, in our case with a duty cycle of 50 %. In this mode of operation there is enough time between bursts for crystal growth and settling on the cellulose surface; also energy release in bursts favors reaction mixture thermalization preventing liquid overheating. Finally, fibers were washed with distilled water and dried at 60 °C for 12 h. Table 1 shows our factorial experimental design.

Fiber characterization

FESEM images were taken on a FEI QUANTA FEG 650 (Hillsboro, OR USA) equipped with a Large Field Detector; samples were coated with a thin layer of carbon before imaging and the micrographs were taken at 10 kV. Elemental analysis, using an energy-dispersive X-ray spectroscopy (EDX) accessory attached to the microscope, was performed at 20 kV. X-ray diffraction (XRD) analyses of clean, cationized fibers and ZnO–fique biocomposites were performed on a Bruker D8 DISCOVER X-ray diffractometer (Madison, WI, USA) with a DaVinci geometry, using a CuKα1 radiation source (40 kV and 30 mA), an area detector VANTEC-500, and a poly(methyl methacrylate) sample holder. The amount of Na and Zn on the fiber's surface after cationization and ZnO deposition was determined by X-ray fluorescence (XRF) spectrometry on a BRUKER S8 TIGER wavelength dispersive XRF spectrometer (Madison, WI, USA) fitted with a high intensity Rh tube (4 kW), scintillation and flow counters for heavy and light elements, and a high precision mechanical goniometer for θ and 2θ measurements. Quantitative analysis was performed using the Quant-Express™ multi-purpose calibration package. X-ray photoelectron spectroscopy (XPS) spectra were obtained on a Surface Science Instruments model SSX-100 (Sunnyvale, CA, USA) using a monochromated Al Kr X-ray source. For attenuated total reflectance (ATR-IR)

Table 1 Experimental design for the fique–ZnO biocomposite synthesis

		Molar ratio $[OH^-]/[Zn^{2+}]$		
		20:1	10:1	4:1
Sonochemical energy				
Time (min)	20	U1	U3	U5
	40	U2	U4	U6
Thermal energy				
Time (min)	60	H1	H3	H5
	120	H2	H4	H6

measurements a Bruker Tensor 27 (Billerica, MA USA) FTIR instrument equipped with a Platinum Diamond ATR unit A225/Q (Billerica, MA, USA) was used at a resolution of 2 cm^{-1} and 32 scans were accumulated for each spectrum. After each synthesis, the remaining solution was tested to detect ZnO particles in solution via UV–Vis spectroscopy at 360 nm, using a Thermo Scientific GENESYS 10S UV–Vis spectrophotometer (Waltham, MA USA) equipped with a Xenon flash lamp.

Results and discussion

Fiber pretreatment

In previous reports from our group we have described the origin and structure of fique fibers (Castellanos et al. 2012; Chacón-Patiño et al. 2013). Fique fibers are extracted from *Furcraea* spp. plants via a mechanical process using a decorticator. The fibers are primarily composed of cellulose, hemicellulose and lignin, with cellulose as the main component (Morán et al. 2007). Figure 1a, depicts a longitudinal view of an individual fique fiber, consisting of elementary cellulose fibrils held together by hemicellulose and lignin. The surface of fique fibers has a heterogeneous morphology, making them attractive matrices for nanomaterials synthesis due to its irregularity and the stabilizing effect of hydroxyl groups in the fibeŕs surface (Dong and Hinestroza 2009).

Initially we attempted to use clean fique fibers as matrices for ZnO synthesis with poor results. We expected that the overall negative surface of the fiber, caused by the high electron density of –OH groups from cellulose, would suffice to retain Zn^{2+} ions and to serve as matrix for ZnO nucleation and growth. Although we observed ZnO crystal formation in the fiber surface, the crystals had a random size distribution, and no definite shape (see supplementary information). Previous work using cellulosic substrates has shown that for the in situ synthesis of transition metal oxides on cellulose, an initial activation of the fiber surface is fundamental to ensure effective metal cation attachment via electrostatic interactions (Dong and Hinestroza 2009; Wang et al. 2010; Chacón-Patiño et al. 2013). Thus, for the synthesis of ZnO nanoparticles we modified the fiber's surface by inducing the formation of $CH_2O^-Na^+$ groups. Because of the high reactivity of the primary OH at C-6 and the absence of steric hindrance, $CH_2O^-Na^+$ groups are readily formed mainly at this position when using an acid/basic treatment, see the "Experimental" section for details (Heinze 2004; Dong and Hinestroza 2009; Shateri Khalil-Abad et al. 2009). XRF analysis of raw, clean and cationized fibers shows the dynamics of Na content during the pretreatment (see supplementary information). Raw fibers contain small amounts of Na (<0.01 %) that is removed, together with other cations such as Ca^{2+}, during the initial ultrasound-cleaning step. After the cationization reaction, the amount of Na^+ in the fiber surface increases up to 2.39 %. This material hence becomes an effective cation exchanger, especially for small transition metal ions such as Zn^{2+}. Sodium ions (hydrated radius: 1.02 Å) in the surface of the activated cellulose could be easily replaced by zinc ions with a smaller hydrated radii (hydrated radius: 0.74 Å; Persson 2010). We used these modified fibers (cationized celluose) as solid supports for the synthesis of ZnO throughout all our experiments.

On the other hand, the fiber cleaning and cationization processes not only increased the amount of sodium ions on the surface, but also helped with the removal of hemicellulose and lignin. Figure 1 shows the fiber's surface before (a) and after (b) the cationization process. FESEM images indicate that after fiber cationization individual microfibrils become evident, due to the removal of hemicellulose and lignin hence increasing surface's area and heterogeneity. Thus after cationization, the cellulosic substrates surface is much more exposed facilitating the the synthesis and stabilization of particles. IR spectra of raw and cationic fibers (Fig. 1c) show typical signals for cellulose, the main component of fique fibers, located at 3300, 2890 and 1030 cm^{-1}. These signals correspond to the vibration of O–H, H–C–H and C–O–C (glycosidic linkage) groups of cellulose, respectively (Morán et al. 2007; Chen et al. 2011; Iskalieva et al. 2012). Interestingly IR spectra also show that cationized fibers lack signals at 1733 and 1239 cm^{-1} related to C=O groups in lignin and hemicellulose and to the aromatic skeletal vibration in lignin (Abraham et al. 2011; Ramadoss and Muthukumar 2014). Absence of lignin and hemicellulose signals indicates partial removal of these materials during the cationization process.

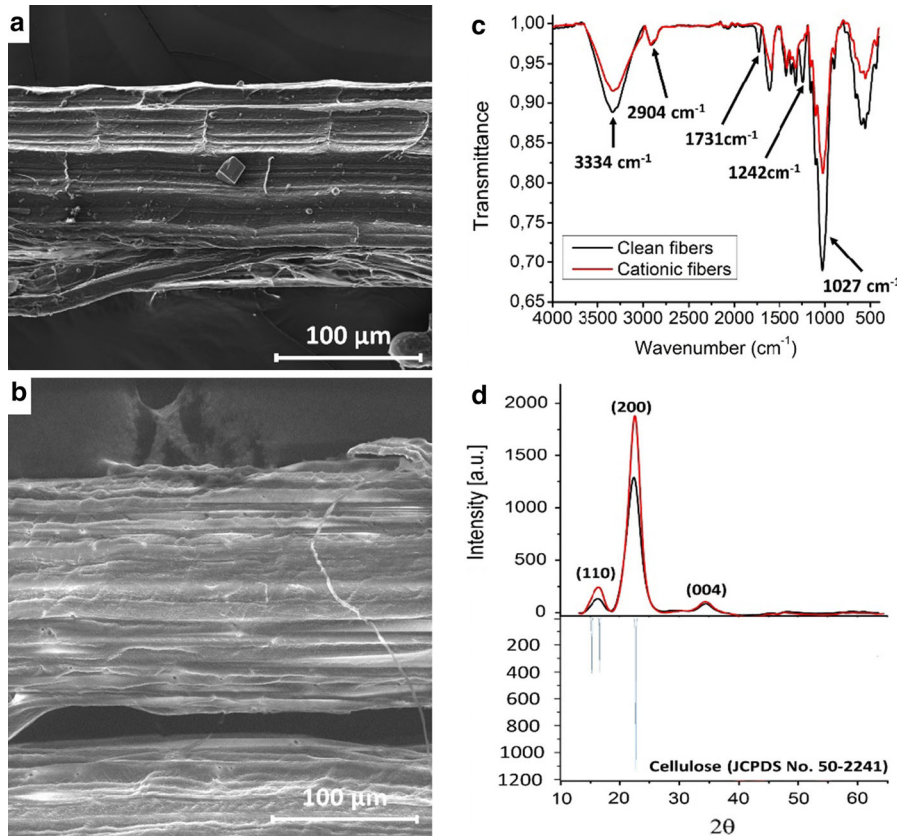

Fig. 1 FESEM micrographs of **a** clean and **b** cationic fibers; **c** IR and **d** DRX spectra of clean and cationic fibers

DRX patterns for clean and cationic fique fibers (Fig. 1d) show three well-defined signals around 16.5°, 22° and 35° corresponding to (1 1 0), (2 0 0) and (0 0 4) planes characteristic of native cellulose (Joint Committee on Powder Diffraction Standards, JCPDS file, no. 50-2241), space group $P2_1$ (No. 4) (Sèbe et al. 2012; French 2013).We also used DRX analysis to establish whether or not the cellulose structure changed after the initial fiber treatment. The cellulose degree of crystallinity (C_I) was calculated according to the following formula (Chen et al. 2011; Luzi et al. 2014):

$$C_I\,(\%) = \frac{I_{Crystalline} - I_{Amorphous}}{I_{Crystalline}} \times 100$$

where $I_{Crystalline}$ is the maximum intensity of diffraction of the (0 0 2) plane at an angle of around 22° and $I_{Amorphous}$ is the intensity of diffraction of the amorphous material, usually taken at an angle between 18° and 19°, where the intensity is at a minimum. According to our data C_I values for clean and cationic fibers were 66.9 and 74.32 %, respectively; indicating an increase in the percentage of crystallinity originated by the removal of amorphous materials (hemicellulose and lignin) during the cationization process.

Synthesis of ZnO–fique biocomposites

Typically, ZnO synthesis in aqueous solution occurs through the following path (Dutta et al. 2012; Katepetch et al. 2013):

$$ZnSO_4 \rightarrow Zn^{2+} + SO_4^{2-} \quad (1)$$

$$NaOH \rightarrow Na^{+} + OH^{-} \quad (2)$$

$$Zn^{2+} + 4OH^{-} \rightleftharpoons Zn(OH)_2 + 2OH^{-} \rightleftharpoons Zn(OH)_4^{2-} \quad (3)$$

$$Zn(OH)_2 \rightarrow ZnO + H_2O \quad (4)$$

$$Zn(OH)_4^{2-} \rightarrow ZnO + H_2O + 2OH^{-} \quad (5)$$

Our synthetic methodology uses a co-precipitation approach in which ZnO particles are formed simultaneously in solution and in the solid phase (cationized fique fibers). Regardless of experimental conditions, in all our experiments we obtained a characteristic milky solution upon ZnO formation in the aqueous phase (Li et al. 2009; Hu et al. 2010). The fibers on the other hand showed no alteration in color (Perelshtein et al. 2009; Katepetch et al. 2013). Analysis of the remnant liquid phase after reaction completion allowed us to observe the effect of different reaction conditions on the free ZnO particles in solution. Initially we followed the reaction dynamics by UV–Vis using a characteristic band, centered at around 360 nm, for ZnO particles in solution (Azizian-Kalandaragh et al. 2009; Patil et al. 2012). Figure 2a, b show plots correlating the absorbance in solution at 360 nm for experiments carried out under different experimental conditions (different $[OH^-]/[Zn^{2+}]$ molar ratios and energy source for $Zn(OH)_n^{(2-n)} \gg$ ZnO hydrolysis). From Fig. 2 it is obvious that the reaction's driving force, either thermal or sonochemical, appears not to have any bearing in the amount of ZnO dispersed in the reaction solution. We observe, for both sonochemical and thermal methods, the same trends in absorbance with high absorbance at low $[OH^-]/[Zn^{2+}]$ ratios and low absorbance at high $[OH^-]/[Zn^{2+}]$ ratios. High absorbance values correspond to increasing amounts of ZnO in solution, while low values indicate lesser amounts of ZnO dispersed in the solution (Link and El-Sayed 1999). Molar $[OH^-]/[Zn^{2+}]$ ratios of 4:1, 10:1 and 20:1 were chosen according to reports by Liu and Zeng, who studied the influence of this parameter on ZnO formation in aqueous phase. These authors found molar ratios ranging from 4:1 to 30:1 as adequate for ZnO nanoparticle formation (Liu and Zeng 2004); however, we did not include molar ratios above 20:1 in our experiments because more recently Kawano et al. reported $[OH^-]/[Zn^{2+}]$ ratios above 25:1 as unsuitable for ZnO nanoparticle formation in solution due to the high solubility of ZnO under very basic conditions (Kawano and Imai 2006). Likewise in Fig. 2, high amounts of ZnO particles at low $[OH^-]/[Zn^{2+}]$ molar ratios can be rationalized in terms of ZnO solubility, which is strongly dependant on pH. For instance ZnO is stable at pH values from 9 to 13, so when higher $[OH^-]/[Zn^{2+}]$ molar ratios are used, the pH increases to a level where ZnO crystallization is hard to achieve (Yamabi and Imai 2002). In addition, longer reaction times result in increasing absorbance values for both thermal and sonochemical methods. Longer reaction times influence the $Zn(OH)_n^{(2-n)} \gg$ ZnO decomposition reactions kinetics resulting in higher amounts of ZnO in solution.

With regards to ZnO deposition onto fique fibers we began by measuring the effective amount of Na and Zn on the fiber surface, by XRF, after exposing the fibers to experimental conditions shown in Table 1. Complete XRF results are provided in the supplementary material section. When using cationic fibers (2.39 % Na) as starting materials we observed that Na^+ exchange was apparently independent of experimental conditions. Table 2 shows, for the ultrasound-assisted synthesis using 750 W, 20 kHz waves, Na^+ exchange average percentages of 56.5 ± 4.4 and 51.5 ± 8.4 % for 20 and 40 min of irradiation, respectively. For the thermal-driven synthesis at 60 °C, Na^+ exchange

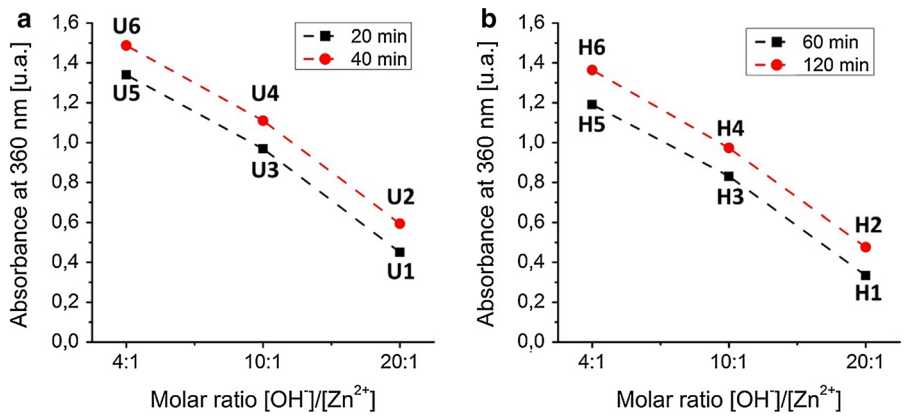

Fig. 2 Variation in UV–Vis absorbance at 360 nm as measured in the reaction aqueous phase, for ZnO nanoparticle synthesis using **a** sonochemical and **b** thermal energy

Table 2 Na^+ exchange (%) on cationized fibers after ZnO synthesis

Test		Na % exchange	
Sonochemical energy 20 kHz, 750 W			
20 min	U1	52.3	56.5 ± 4.4
	U3	56.1	
	U5	61.1	
40 min	U2	59.8	51.5 ± 8.4
	U4	43.1	
	U6	51.5	
Thermal energy 60 °C			
60 min	H1	63.6	54.5 ± 8.1
	H3	48.1	
	H5	51.9	
120 min	H2	58.2	51.2 ± 6.9
	H4	44.4	
	H6	51.0	

average percentages were 54.5 ± 8.1 and 51.2 ± 6.9 % for experiments using 60 and 120 min of reaction time, respectively.

In contrast, the amount of Zn on the fiber's surface is strongly dependent on experimental conditions. Figure 3 shows the trends in Zn content measured by XRF (complete XRF characterization is provided in the supplementary material section). For the ultrasound-assisted synthesis both irradiation time and $[OH^-]/[Zn^{2+}]$ ratios do influence Zn deposition onto the fiber's surface. An irradiation time of 40 min favors Zn deposition (1.06 %) while 20 min exposures yields less Zn (0.93 %) on the surface, for a $[OH^-]/[Zn^{2+}]$ ratio of 4:1. Although the same trend is observed for the thermal-driven synthesis, heating time has a weaker effect in Zn deposition when compared to ultrasound. For instance a heating time of 120 min favors Zn deposition (0.41 %) over 60 min (0.35 %) for $[OH^-]/[Zn^{2+}]$ ratio 4:1. For the synthesis of ZnO particles, an activation energy is essential since the process is thermodynamically unfavorable (Katepetch et al. 2013). The activation energy was provided in this study by ultrasonic or heating treatments (Yang and Yang 2010). Sonochemical irradiation seems to have a stronger effect on Zn deposition because it induces cavitation which in turns produces localized heating and high pressure pockets in the reaction media (Yadav et al. 2008). Cavitation has a significant impact on particle synthesis in heterogeneous systems than in homogeneous ones; shock waves and micro jets, created when cavitation bubbles collapse, not only promote particle adhesion to the solid support but also improve their distribution on its surface (Perelshtein et al. 2009). The overall effect is observed as abundant and well-dispersed ZnO particles on the fiber's surface when using ultrasound energy, which is not the case when using the heating method.

We also observed an inverse relationship between $[OH^-]/[Zn^{2+}]$ molar ratios and the amount of Zn deposited on the fiber (Fig. 3). For both heating and irradiation methods a $[OH^-]/[Zn^{2+}]$ molar ratio of 4:1 (experiments U5, U6, H5, H6) always produced the highest amount of Zn on the fibers. These results are in accordance with UV–Vis observations of the reaction aqueous phase as discussed above (Fig. 2). Basically, high $[OH^-]/[Zn^{2+}]$ molar ratios decrease ZnO deposition regardless of the source of the energy used to drive the reaction. This effect can be understood in terms of slower rates of ZnO formation compared to

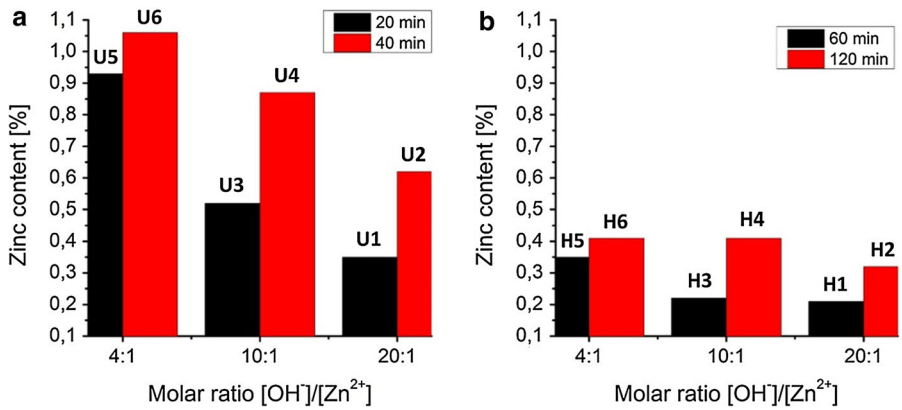

Fig. 3 XRF measurements of ZnO deposition on cellulosic fibers, driven by **a** sonochemical and **b** thermal energy

dissolution rates at high OH^- concentrations (Liu and Zeng 2004).

ZnO–fique biocomposite characterization

Figure 4 shows XRD and XPS spectra for the ZnO–fique biocomposite. In addition to signals at 22° and 35° corresponding to (2 0 0) and (0 0 4) planes of native cellulose, the XRD diffractogram in Fig. 4a shows peaks at 31°, 34°, 36°, 47°, 56° and 62° characteristic of (1 0 0), (0 0 2), (1 0 1), (1 0 2), (1 1 0) and (1 0 3) planes of hexagonal ZnO, respectively. These patterns correspond to zincite (JCPDS file, no. 36-1451, space group $P6_3mc$, No. 186), and do confirm the presence of ZnO on the surface of the cellulosic substrate (Asar et al. 2012; Lin et al. 2014).

Figure 4b shows the full XPS spectrum of the ZnO-fique fiber biocomposite where binding energies were calibrated according to the signal for adventitious carbon (284.8 eV). The XPS spectrum shows high intensity peaks at binding energies of 284.8, 531.9, 1022.6 and 1044.6 eV, corresponding to C 1s, O 1s, Zn $2p_{3/2}$ and Zn $2p_{1/2}$, respectively. Characteristic signals for Zn (Zn $2p_{1/2}$ and Zn $2p_{3/2}$) in the XPS spectrum indicate the presence of ZnO particles on the fiber surface; the chemical valence (oxidation state) of Zn in the ZnO crystals is +2 (Yao et al. 2012; Katepetch et al. 2013; Al-Gaashani et al. 2013).

With spectroscopic analysis effectively indicating the presence of ZnO on the fiber surface, we performed FE-SEM measurements to assert the morphology and distribution of the material. It is well known that ZnO crystal shapes determine the materials' use and application, especially in the field of optoelectronics. Relative growth rates of ZnO crystal facets, form a wide variety of crystal shapes that can be altered by the concentration of ions (anions mostly), the reaction conditions and the presence of active surfaces. Laser vaporization, electrodeposition or physical vapor deposition at high temperature are typically used to grow aligned ZnO structures on solid substrates such as metal nitride films and semiconductor films. These methods are expensive and time consuming. On the other hand many approaches for the synthesis of nanostructured zinc oxide in solution, using both thermal and ultrasound energy as the driving force, are found in literature. Most solution-phase synthesis produce one-dimensional ZnO particles with spherical, amorphous or rod-like morphology depending on synthetic conditions (Becheri et al. 2007; Azizian-Kalandaragh et al. 2009; Hu et al. 2010; Patil et al. 2012; Katepetch et al. 2013; Lin et al. 2014). The synthetic method described in this manuscript takes advantage of simple wet chemistry to produce two-dimensional ZnO microstructures on a cellulosic substrate.

Based on previous results, we can ascertain that reaction time, driving force and $[OH^-]/[Zn^{2+}]$ molar ratios influence the deposition of ZnO on cellulosic fibers. In order to assess the effect of those variables on shape, distribution and morphology of deposited crystals we imaged the specimens via FESEM. Figure 5 shows FESEM images of ZnO–fique fiber biocomposites where the crystal's structure, size and distribution of ZnO particles on the fiber surface vary widely. As a common feature, in our experiments ZnO particles exhibit defined shapes regardless of the reaction driving force. In most cases we observe flower-like micrometer-sized structures composed of nanometer-sized units such as needles, rods or

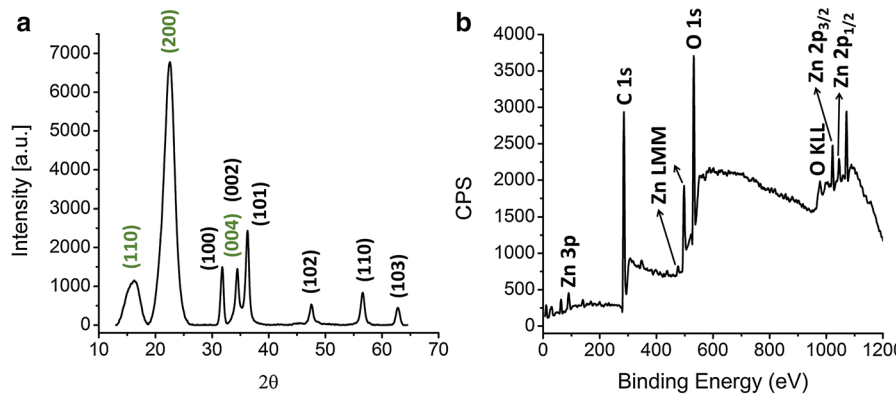

Fig. 4 **a** XRD of biocomposites, **b** XPS of biocomposites

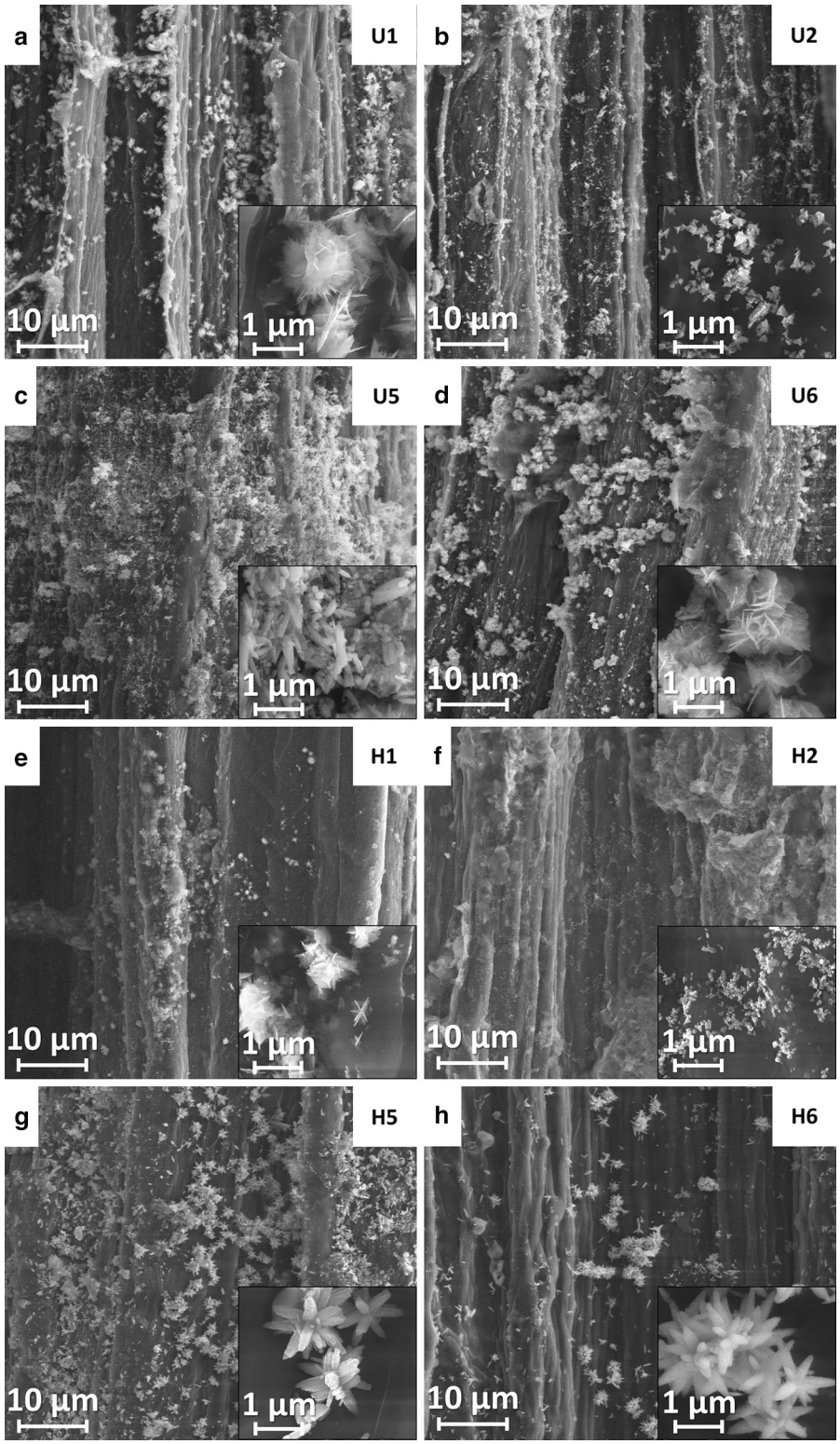

Fig. 5 FE-SEM micrographs of ZnO–fique fiber biocomposites. **a** U1, **b** U2, **c** U5, **d** U6, **e** H1, **f** H2, **g** H5, **h** H6

platelets (Cheng et al. 2008; Li et al. 2009; Wang et al. 2013; Kuriakose et al. 2013). This observation is opposite to some reports stating that near-spherical structures are produced when using thermal energy (Li et al. 2009) in homogeneous phase reactions. As a common feature $[OH^-]/[Zn^{2+}]$ molar ratios of 4:1 (experiments U5, U6, H5, H6) produced thickly arranged micro clusters with a variety of morphologies, formed mainly by rod-shaped and scale-shaped ZnO nanocrystals. For instance samples H5 and H6 (Fig. 5g, h), where the driving force of the reaction was thermal, exhibit flower-like microstructures composed of nanorods. These structures, the most typical for ZnO, are formed when the crystal grows along the [001] direction. Growth in the [001] direction is rationalized in terms of $Zn(OH)_4^{2-}$ ion formation, due to the high pH in the reaction media; these ions in turn can react with OH^- groups attached to the initial ZnO clusters, allowing growth in the [001] direction (Al-Gaashani et al. 2013). Similar results were obtained by Jaber and Laânab who also reported rod-like shapes for ZnO nanoparticles synthesized at 60 °C, with a $[OH^-]/[Zn^{2+}]$ molar ratio of 2.5:1 (Jaber and Laânab 2014). In addition short heating times (60 min, sample H5) seem to have a positive effect in ZnO crystals distribution on the fiber surface, in contrast with longer heating times (120 min, sample H6) which produced less uniform distributions. No differences in crystal's shapes and arrangements were observed between samples H5 an H6.

Samples U5 and U6 (Fig. 5c, d), where the driving force of the reaction was sonochemical, exhibit thick clusters of ZnO nanorods (U5) and flower-like microstructures composed of platelets (U6). There is a dramatic change in ZnO morphology as one move from 20 to 40 min for ultrasound-assisted reaction times. At 20 min of reaction (U5) ZnO nanorods of different sizes are present in the fiber's surface. As the reaction time increases to 40 min (U6) ZnO particles undergo a morphological evolution from nanorods to nanoplatelets clustered in flower-like structures. These results are similar to reports by Khorsand et al. indicating that ZnO morphology changes, from amorphous particles to nanorods and from nanorods to flower-like structures, as reaction time increases (Zak et al. 2013). In addition FESEM also shows a significant influence of the reaction's driving force on the distribution of ZnO crystals on the fiber surface. Samples U5 and U6 exhibit surfaces over-saturated by clusters and layers of ZnO crystals, these samples also exhibit the highest amounts of Zn (0.93 % for U5 and 1.05 % for U6) according to XRF results (Fig. 3). On the other hand, samples H5 and H6 show a more uniform distribution of flower-like structures with Zn contents of 0.35 and 0.41 %, respectively (Fig. 3).

In contrast to $[OH^-]/[Zn^{2+}]$ molar ratios of 4:1, where particles with a variety of morphologies were formed (experiments U5, U6, H5, H6), $[OH^-]/[Zn^{2+}]$ molar ratios of 20:1 (experiments U1, U2, H1, H2) always produced ZnO nanoplatelets (Fig. 5a, b, e, f) regardless of the reaction's driving force. For shorter reaction times (U1, 20 min, and H1, 60 min) nanoplatelets were assembled in flower-like structures. Kuriakose et al. reported that the growth of nanoplatelets in flower-like structures involves an initial formation of spherical nanoparticles, followed by an oriented attachment of ZnO nanoparticles to form nanoplatelets. The nanoplatelets finally self-assemble into flower-like structures to minimize their surface energy (Ye et al. 2006; Kuriakose et al. 2013). When longer reaction times were used (U2, 40 min, and H2, 120 min) the flower-like arrangements appear disrupted and only individual nanoplatelets remain on the fiber surface. Although FESEM shows similar results for the crystal morphology of ZnO when using $[OH^-]/[Zn^{2+}]$ molar ratios of 20:1 regardless of reaction driving force, it also indicates a significant difference in the ZnO crystals' distribution. It is clear that use of sonochemical energy has a positive effect on ZnO crystals distribution on the fiber surface. XRF results also support this observation, as more ZnO is deposited under experimental conditions U1 (0.35 %) and U2 (0.62 %) than under experimental conditions H1 (0.22 %) and H2 (0.33 %; Fig. 3). Finally, it appears that the formation of different ZnO crystal shapes is controlled by $[OH^-]/[Zn^{2+}]$ molar ratios and the driving force of the reaction (only at low $[OH^-]/[Zn^{2+}]$ ratios); although the last one seems to also have a stronger effect on ZnO crystal distribution on the fiber surface (Cao and Cai 2008).

Conclusions

ZnO nanoparticles were successfully synthesized on the surface of fique fibers using thermal and sonochemical methods. It was found that the sonochemical method usually produced higher amounts of ZnO on the fibers

surface. We also observed that the initial fiber cationization process is essential to efficiently synthesize ZnO particles onto the cellulosic substrate. We also observed that the $[OH^-]/[Zn^{2+}]$ ratio and the heating/sonication time strongly influenced the amount, shape, size and distribution of ZnO crystals on the cellulosic surface of fique fibers. The fact that diverse morphologies and size distributions were achieved under different experimental conditions confirms the potential of fique fibers as nanoreactors for the synthesis of nanomaterials. Since fique fibers are mechanically strong and can be easily transformed into woven mats and fibrous-based products, it is feasible to think that these functionalized materials can be used as filtration media as well as beds in catalytic process or in the production of smart textiles and fibers. We are currently testing these materials for the photocatalytic degradation of pollutants, such as dyes and pesticides, which will be the topic of a forthcoming publication.

Acknowledgments We acknowledge funding from COLCIENCIAS and the World Bank (Grant RC No. 0373). We also thank Guatiguará Technology Park, the Central Research Laboratory Facility and the X-ray diffraction and electron microscopy laboratories at Universidad Industrial de Santander for infrastructural support.

References

Abraham E, Deepa B, Pothan LA et al (2011) Extraction of nanocellulose fibrils from lignocellulosic fibres: a novel approach. Carbohydr Polym 86:1468–1475

Al-Gaashani R, Radiman S, Daud AR et al (2013) XPS and optical studies of different morphologies of ZnO nanostructures prepared by microwave methods. Ceram Int 39:2283–2292. doi:10.1016/j.ceramint.2012.08.075

Asar N, Erol A, Okur S, Arikan MC (2012) Morphology-dependent humidity adsorption kinetics of ZnO nanostructures. Sens Actuators A Phys 187:37–42. doi:10.1016/j.sna.2012.08.019

Azizian-Kalandaragh Y, Khodayari A, Behboudnia M (2009) Ultrasound-assisted synthesis of ZnO semiconductor nanostructures. Mater Sci Semicond Process 12:142–145. doi:10.1016/j.mssp.2009.09.006

Barua S, Das G, Aidew L et al (2013) Copper–copper oxide coated nanofibrillar cellulose: a promising biomaterial. RSC Adv 3:14997–15004. doi:10.1039/c3ra42209g

Becheri A, Dürr M, Lo Nostro P, Baglioni P (2007) Synthesis and characterization of zinc oxide nanoparticles: application to textiles as UV-absorbers. J Nanopart Res 10:679–689. doi:10.1007/s11051-007-9318-3

Cao B, Cai W (2008) From ZnO nanorods to nanoplates: chemical bath deposition growth and surface-related emissions. J Phys Chem C 112:680–685. doi:10.1021/jp076870l

Castellanos LJ, Blanco-Tirado C, Hinestroza JP, Combariza MY (2012) In situ synthesis of gold nanoparticles using fique natural fibers as template. Cellulose 19:1933–1943. doi:10.1007/s10570-012-9763-8

Chacón-Patiño ML, Blanco-Tirado C, Hinestroza JP, Combariza MY (2013) Biocomposite of nanostructured MnO2 and fique fibers for efficient dye degradation. Green Chem 15:2920. doi:10.1039/c3gc40911b

Chen W, Yu H, Liu Y et al (2011) Isolation and characterization of cellulose nanofibers from four plant cellulose fibers using a chemical-ultrasonic process. Cellulose 18:433–442. doi:10.1007/s10570-011-9497-z

Chen S, Zhou B, Hu W et al (2013) Polyol mediated synthesis of ZnO nanoparticles templated by bacterial cellulose. Carbohydr Polym 92:1953–1959. doi:10.1016/j.carbpol.2012.11.059

Cheng JP, Zhang XB, Luo ZQ (2008) Oriented growth of ZnO nanostructures on Si and Al substrates. Surf Coat Technol 202:4681–4686. doi:10.1016/j.surfcoat.2008.03.032

Dong BH, Hinestroza JP (2009) Metal nanoparticles on natural cellulose fibers: electrostatic assembly and in situ synthesis. ACS Appl Mater Interfaces 1:797–803. doi:10.1021/am800225j

Dutta K, Das S, Pramanik A (2012) Concomitant synthesis of highly crystalline Zn-Al layered double hydroxide and ZnO: phase interconversion and enhanced photocatalytic activity. J Colloid Interface Sci 366:28–36. doi:10.1016/j.jcis.2011.09.081

Faruk O, Bledzki AK, Fink H-P, Sain M (2012) Biocomposites reinforced with natural fibers: 2000–2010. Prog Polym Sci 37:1552–1596. doi:10.1016/j.progpolymsci.2012.04.003

French AD (2013) Idealized powder diffraction patterns for cellulose polymorphs. Cellulose 21:885–896. doi:10.1007/s10570-013-0030-4

Galland S, Andersson RL, Salajková M et al (2013) Cellulose nanofibers decorated with magnetic nanoparticles—synthesis, structure and use in magnetized high toughness membranes for a prototype loudspeaker. J Mater Chem C 1:7963. doi:10.1039/c3tc31748j

Gañán P, Mondragon I (2002) Surface modification of fique fibers. Effect on their physico-mechanical properties. Polym Compos 23:383–394. doi:10.1002/pc.10440

Gaya UI, Abdullah AH, Hussein MZ, Zainal Z (2010) Photocatalytic removal of 2,4,6-trichlorophenol from water exploiting commercial ZnO powder. Desalination 263:176–182. doi:10.1016/j.desal.2010.06.055

Heinze T (2004) Chemical functionalization of cellulose. In: Dumitriu S (ed) Polysaccharides: structural diversity and functional versatility, 2nd edn. CRC Press, United States of America, pp 551–590. doi:10.1201/978120030822

Hu QR, Wang SL, Jiang P et al (2010) Synthesis of ZnO nanostructures in organic solvents and their photoluminescence properties. J Alloys Compd 496:494–499. doi:10.1016/j.jallcom.2010.02.086

Iskalieva A, Yimmou BM, Gogate PR et al (2012) Cavitation assisted delignification of wheat straw: a review. Ultrason Sonochem 19:984–993. doi:10.1016/j.ultsonch.2012.02.007

Jaber B, Laânab L (2014) One step synthesis of ZnO nanoparticles in free organic medium: structural and optical characterizations. Mater Sci Semicond Process 27:446–451. doi:10.1016/j.mssp.2014.07.025

John M, Thomas S (2008) Biofibres and biocomposites. Carbohydr Polym 71:343–364. doi:10.1016/j.carbpol.2007.05.040

Katepetch C, Rujiravanit R, Tamura H (2013) Formation of nanocrystalline ZnO particles into bacterial cellulose pellicle by ultrasonic-assisted in situ synthesis. Cellulose 20:1275–1292. doi:10.1007/s10570-013-9892-8

Kawano T, Imai H (2006) Fabrication of ZnO nanoparticles with various aspect ratios through acidic and basic routes. Cryst Growth Des 6:1054–1056. doi:10.1021/cg050338a

Khorsand Zak A, Majid WHA, Wang HZ et al (2013) Sonochemical synthesis of hierarchical ZnO nanostructures. Ultrason Sonochem 20:395–400. doi:10.1016/j.ultsonch.2012.07.001

Kuriakose S, Bhardwaj N, Singh J et al (2013) Structural, optical and photocatalytic properties of flower-like ZnO nanostructures prepared by a facile wet chemical method. Beilstein J Nanotechnol 4:763–770. doi:10.3762/bjnano.4.87

Li X, Tabil LG, Panigrahi S (2007) Chemical Treatments of Natural Fiber for Use in Natural Fiber-Reinforced Composites: a Review. J Polym Environ 15:25–33. doi:10.1007/s10924-006-0042-3

Li H, Ni Y, Hong J (2009) Ultrasound-assisted preparation, characterization and properties of flower-like ZnO microstructures. Scr Mater 60:524–527. doi:10.1016/j.scriptamat.2008.11.047

Lin S-T, Thirumavalavan M, Jiang T-Y, Lee J-F (2014) Synthesis of ZnO/Zn nano photocatalyst using modified polysaccharides for photodegradation of dyes. Carbohydr Polym 105:1–9. doi:10.1016/j.carbpol.2014.01.017

Link S, El-Sayed MA (1999) Size and temperature dependence of the plasmon absorption of colloidal gold nanoparticles. J Phys Chem B 103:4212–4217. doi:10.1021/jp984796o

Liu B, Zeng HC (2004) Room temperature solution synthesis of monodispersed single-crystalline ZnO nanorods and derived hierarchical nanostructures. Langmuir 20:4196–4204. doi:10.1021/la035264o

Luzi F, Fortunati E, Puglia D et al (2014) Optimized extraction of cellulose nanocrystals from pristine and carded hemp fibres. Ind Crops Prod 56:175–186. doi:10.1016/j.indcrop.2014.03.006

Morán JI, Alvarez VA, Cyras VP, Vázquez A (2007) Extraction of cellulose and preparation of nanocellulose from sisal fibers. Cellulose 15:149–159. doi:10.1007/s10570-007-9145-9

Ovalle SA, Blanco-Tirado C, Combariza MY (2014) Síntesis in situ de nanopartículas de plata sobre fibras de fique. Rev Colomb Química 42:30–37

Patil AB, Patil DS, Bhanage BM (2012) ZnO nanoparticle by solar energy and their catalytic application for α-amino phosphonates synthesis. Mater Lett 86:50–53. doi:10.1016/j.matlet.2012.07.009

Perelshtein I, Applerot G, Perkas N et al (2009) Antibacterial properties of an in situ generated and simultaneously deposited nanocrystalline ZnO on fabrics. ACS Appl Mater Interfaces 1:361–366. doi:10.1021/am8000743

Persson I (2010) Hydrated metal ions in aqueous solution: how regular are their structures? Pure Appl Chem 82:1901–1917. doi:10.1351/PAC-CON-09-10-22

Ramadoss G, Muthukumar K (2014) Ultrasound assisted ammonia pretreatment of sugarcane bagasse for fermentable sugar production. Biochem Eng J 83:33–41. doi:10.1016/j.bej.2013.11.013

Sèbe G, Ham-Pichavant F, Ibarboure E et al (2012) Supramolecular structure characterization of cellulose II nanowhiskers produced by acid hydrolysis of cellulose I substrates. Biomacromolecules 13:570–578. doi:10.1021/bm201777j

Selvam NCS, Narayanan S, Kennedy LJ, Vijaya JJ (2013) Pure and Mg-doped self-assembled ZnO nano-particles for the enhanced photocatalytic degradation of 4-chlorophenol. J Environ Sci 25:2157–2167. doi:10.1016/S1001-0742(12)60277-0

Shateri Khalil-Abad M, Yazdanshenas ME, Nateghi MR (2009) Effect of cationization on adsorption of silver nanoparticles on cotton surfaces and its antibacterial activity. Cellulose 16:1147–1157. doi:10.1007/s10570-009-9351-8

Wang H, Zheng M, Chen J et al (2010) Synthesis of MnO2 microfiber with secondary nanostructure by cotton template. J Nanotechnol 2010:1–5. doi:10.1155/2010/479172

Wang M, Zhang Y, Zhou Y et al (2013) Rapid room-temperature synthesis of nanosheet-assembled ZnO mesocrystals with excellent photocatalytic activity. CrystEngComm 15:754. doi:10.1039/c2ce26660a

Xue C-H, Chen J, Yin W et al (2012) Superhydrophobic conductive textiles with antibacterial property by coating fibers with silver nanoparticles. Appl Surf Sci 258:2468–2472. doi:10.1016/j.apsusc.2011.10.074

Yadav RS, Mishra P, Pandey AC (2008) Growth mechanism and optical property of ZnO nanoparticles synthesized by sonochemical method. Ultrason Sonochem 15:863–868. doi:10.1016/j.ultsonch.2007.11.003

Yamabi S, Imai H (2002) Growth conditions for wurtzite zinc oxide films in aqueous solutions. J Mater Chem 12:3773–3778. doi:10.1039/b205384e

Yang YH, Yang GW (2010) Temperature dependence and activation energy of ZnO nanowires grown on amorphous carbon. Chem Phys Lett 494:64–68. doi:10.1016/j.cplett.2010.05.074

Yao L, Zheng M, Li C et al (2012) Facile synthesis of superhydrophobic surface of ZnO nanoflakes: chemical coating and UV-induced wettability conversion. Nanoscale Res Lett 7:216. doi:10.1186/1556-276X-7-216

Ye C, Bando Y, Shen G, Golberg D (2006) Thickness-dependent photocatalytic performance of ZnO nanoplatelets. J Phys Chem B 110:15146–15151. doi:10.1021/jp061874w